Original Article

Incorporation of Bioactive Glass Nanoparticles in 3D-Printed Acrylic Resin: Impact on Mechanical and Physical Properties: An In Vitro Study

Chawan M. Qader [1*], *Neda Al-Kaisy*[1]

Abstract

Objective: This study aimed to evaluate the effect of incorporating bioactive glass (BAG) nanoparticles at varying concentrations on the mechanical and physical properties of 3D-printed denture base resin. Specifically, flexural strength, surface roughness, and surface hardness.

Methods: Six groups of 3D-printed acrylic resin specimens were studied: one control group (0% BAG) and five experimental groups containing 1%, 1.5%, 2%, 2.5%, and 3% BAG nanoparticles by weight. Flexural strength, surface hardness, and roughness testing were done on 10 specimens. All were digitally planned and 3D printed using SprintRay. XRD, FTIR-ATR, and FESEM were used to characterise the sample. Mechanical testing includes three-point bending for flexural strength, Shore D durometers for surface hardness, and portable roughness testers for surface roughness.

Results: Flexural strength did not differ significantly among groups (ANOVA, $p = 0.527$), with mean values ranging from 130.6 ± 2.4 MPa (control) to 135.5 ± 2.0 MPa (3% BAG). Surface hardness showed significant improvements at 1.5% (89.9 ± 1.2) and 2% (89.9 ± 1.2) compared with the control (88.2 ± 1.6; $p = 0.028$ and $p = 0.020$, respectively). Surface roughness decreased progressively with BAG addition, and the 3% group (0.063 ± 0.017 µm) was significantly smoother than both the control (0.134 ± 0.090 µm; $p = 0.01$) and the 1% group (0.125 ± 0.101 µm; $p = 0.014$).

Conclusions: Incorporating up to 3% BAG nanoparticles into 3D-printed denture base resin can improve surface properties without compromising flexural strength. The concentration between 1.5% and 3% significantly increased the surface hardness and roughness. These advancements imply that BAG-modified resins have the potential to provide advantages such as enhanced clinical longevity and ease of use for prosthetic devices that are manufactured using 3D technology.

Keywords: *Bioactive glass materials, Nanoparticles, Three-dimensional printing, 3D acrylic resin.*

Submitted: August 24, 2025, Accepted: October 9, 2025, Published: December 1, 2025.

Cite this article as: Qader CM, Al-Kaisy N. Incorporation of Bioactive Glass Nanoparticles in 3D-Printed Acrylic Resin: Impact on Mechanical and Physical Properties: An In Vitro Study. Sulaimani Dent J. 2025;12(3):10-20.

DOI: https://doi.org/10.17656/sdj.10212

1. *Department of Prosthodontics, College of Dentistry, University of Sulaimani, Sulaimani, Iraq.*

* *Corresponding author*: *chawan.qadir@univsul.edu.iq.*

Published by the College of Dentistry, University of Sulaiman

Introduction

Three-dimensional (3D) printing is an innovative additive manufacturing method that has been integrated into the dental field, particularly affecting dental esthetics. It enables the production of accurate, comfortable, and aesthetically pleasing prostheses, improving patient outcomes. The adoption of 3D printing in dentistry is gradually increasing due to advantages including diminished production time and costs when compared to the conventional heat-cured acrylic procedure[1,2]. As the demand for chair-side fabrication and same-day delivery of prosthetic appliances increases, it is likely that optimization of printable materials can decrease the use of conventional methods and improve the accessibility of dental care[3].

However, 3D-printed materials often fail to exhibit the mechanical properties of heat-cured PMMA, despite their potential for increased production efficiency and customization. Conventional PMMA exhibited improved flexural strength, impact resistance, and bonding properties[4]. These findings suggest that further development of 3D-printed acrylic resins is necessary to enhance their mechanical and physical properties. Recent comparative work has also shown that 3D-printed denture bases can achieve significantly higher retention values than conventional PMMA bases, emphasizing the functional benefits of additive manufacturing[5].

Nanotechnology has also drawn attention because it is being used to enhance dentistry, particularly in the development of polymer-based products. Nanoparticles are microscopic in size with a large surface area; thus, they can essentially alter the surface and mechanical properties of polymers. The addition of nanofillers to PMMA influences parameters such as bending strength, surface texture, and hardness of the material[6-8].

The incorporation of various nanoparticles and compounds enhances the mechanical and biological properties of the 3D-printed dental acrylic polymers. The best materials to have been used were zirconium dioxide, titanium dioxide, and silver-loaded mesoporous silica nanoparticles. The titanium dioxide nanoparticles increased flexural strength and surface hardness and reduced solubility. Furthermore, they exhibited antifungal efficiency against Candida albicans, especially at doses between 0.10 and 0.50 wt%[9,10]. Zirconium dioxide nanoparticles resulted in enhanced diametral compressive strength, concurrently inducing a reduction in tensile strength, indicating a change in the material's mechanical properties[11]. Silver-loaded mesoporous composites improved surface hardness and crack resistance, and showed potent antifungal activity against *Candida albicans* without significant cytotoxicity[12]. The findings indicate that nanoparticle reinforcement can be utilized to enhance the strength of denture base materials and impart antimicrobial properties.

The performance of these nanofillers is highly affected by concentration, dispersion quality, and surface functionalization. Improvements in mechanical and biological properties may lead to trade-offs, such as alterations in surface roughness and considerations of cytotoxicity[13].

Bioactive glass is regarded as one of the currently available nanomaterials due to its potential bioactivity and clinical advantages. It enhances soft tissue integration, exhibits antimicrobial properties, and promotes bone repair[14]. The controlled dissolution of bioactive glass and the subsequent release of ions can initiate the formation of a hydroxyapatite (HA) layer, which can chemically adhere to living tissues.[15] The extent of this bioactivity is significantly affected by the material's composition and morphology[16,17]. Although these effects were not investigated in the present study, incorporating BAG into 3D-printed resins represents an initial step toward developing biofunctional denture base materials.

To date, BAG has been integrated into composites, glass ionomer cements, and toothpastes,[18] and more recently into 3D printing resins for orthodontic aligners and intraoral devices, where it maintained mechanical strength and exhibited beneficial ion release and biocompatibility[19,20].

However, only a few studies have examined its incorporation into 3D-printed denture base resins, particularly in comparison with conventional heat-cured acrylic resins[20-22]. To the best of our knowledge, the mechanisms by which bioactive nanoparticles interact with 3D-printed acrylic denture bases remain unclear. While the reinforcing effects of bioactive glass have been documented in conventional heat-cured PMMA systems, their incorporation into 3D-printed denture base resins has yet to be comprehensively investigated. This distinction is clinically essential because 3D-printed resins differ in polymerization method and microstructure from conventional PMMA, which may influence nanoparticle interactions and function[23]. Given the growing use of 3D printing in denture manufacturing, it is crucial to assess whether additive manufacturing materials can gain advantages from the incorporation of bioactive glass (BAG).

Therefore, the current study investigates the effect of five different amounts of bioactive glass nanoparticles on the strength, roughness, and hardness of 3D-printed denture base materials. The objective is to determine whether these modifications lead to significant changes

in performance, thereby testing the null hypothesis that they do not.

Materials and methods

Bioactive glass nanoparticle

Bioactive glass nanoparticles (Nanochemazone™, Canada), a GMP and ISO 9001:2015 holding, and Series No. NCZ-RK-243/1224A with a lot size of 300 kg and purity of >99%, a particle size of approximately 100 nm, and a specific surface area ranging from 150 m^2/g, as determined by BET analysis. The composition included SiO_2 (45–55 wt%), CaO (20–30 wt%), Na_2O (10–15 wt%), and P_2O_5 (4–6 wt%), with trace elements ranging from 0.5 to 1 wt%. The bulk density was documented as 1.5 g/cm^3, and the powder exhibited a white to off-white color. This material is certified for dental and bone tissue engineering applications, ensuring biocompatibility.

The study's experimental design

The sample size was calculated using G*Power 3.1 software for a one-way ANOVA (fixed effects, omnibus, one-way), with a significance level (α) of 0.05 and a desired power (1–β) of 0.80. Based on these parameters, the study was powered to detect a medium-to-large effect size (Cohen's $f = 0.335$). A total of 120 specimens were produced via 3D printing, including one control group with pure resin and five experimental groups containing varying concentrations of BAG nanoparticles (1%, 1.5%, 2%, 2.5%, and 3% by weight).

Mixing bioactive glass nanoparticles with 3D acrylic resin

The denture base material used in this study was NextDent 3D printing resin (Vertex Dental, Netherlands). The bioactive glass nanoparticle content was calculated using the known density of liquid NextDent resin (1.20 g/cm^3) to ensure accurate and consistent weight proportions. For a fixed resin volume of 100 cm^3, the total mass was determined to be 120 g. Target concentrations were achieved by applying standard weight percentage formulas to calculate the precise mass of nanoparticles required for each group. Then the resin was manually stirred for 10 minutes in a 400 mL beaker (IWAKI Pyrex®, Japan), followed by the addition of a pre-weighed concentration of nanoparticles measured with a KERN measuring scale (KERN®, Germany) and an ADAM Nimbus scale (Adam Equipment®, USA) with a precision of 0.01 mg (Table 1). The dispersion of nanoparticles is achieved using sonication and vacuum mixing, as effective distribution has been shown to influence the mechanical properties of acrylic nanocomposites[23]. The blend was sonicated for 2 minutes using a Qsonica sonicator (Qsonica, Newtown, CT, USA), stirred for 5 minutes, and then sonicated again for 1 minute. A final five-minute mixing cycle was performed using a Vacuum Power Mixer Plus (Whip Mix, Euro-Vac, USA) to ensure the reproducibility of the preparation method.

While mixing the 3D printing resin with bioactive glass nanoparticles, aluminum foil was used to protect it from ambient light, thereby preventing premature polymerization.

3D-printed denture base resin specimen fabrication

Three-dimensional (3D) model specimens were designed using the Blender for Dental software program (Blender Foundation®), according to ISO 20795-1:2013. Two bar sets were used in the study: 65 × 10 × 3.3 mm for flexural strength testing and 12 × 12 × 3 mm for surface roughness and hardness testing (Fig. 1). The finalized designs were saved as STL (Standard Tessellation Language) files, sliced with adjusted settings, and then exported to the 3D printer.

The samples were printed using a 3D printer (SprintRay®, model SRP2110C). Printing was performed in Turbo mode according to the manufacturer's instructions, using a 100 µm layer thickness and a curing time of 1.5–2 seconds per layer. All samples were printed simultaneously on a single build platform under identical conditions at room temperature for approximately eight minutes.

After the printing process was completed for all of the specimens, they were transferred to the SprintRay Washing Machine. After washing for five minutes in isopropyl alcohol at a concentration of 99%, they were allowed to dry for ten minutes. The final step involved curing the samples under 405 nm blue light in the SprintRay ProCure 2 Curing Machine within 15 minutes. All operations were performed in a setting maintained at 23 ± 2°C and 50 ± 10% relative humidity.

The printed specimens were then manually polished under dry conditions using silicon carbide sandpapers of grits of 400, 600, 800, 1000, and 1500. The application of the individual grits was performed ten times for each grit, and the same operator carried out all finishing operations to ensure standardization. The dimensions of the final samples were checked with a digital caliper to an accuracy of ± 0.1 mm.

Characterization of the specimens

X-Ray Diffraction (XRD) analysis

X-ray diffraction (XRD) examination was performed using an X'Pert PRO diffractometer (Panalytical, Netherlands) equipped with a copper anode, operated at 40 kV and 40 mA. Scanning took place over a 2θ range of 5.01° to 79.97°, utilizing a step size of 0.026°. Diffraction patterns were generated for pure BAG nanoparticles and 3D-printed acrylic resin comprising 3 wt% BAG. The 3% concentration was selected because it showed the most significant nanoparticle mixing in the tested groups, which is optimal for recognizing distinct diffraction peaks and monitoring the dispersion of bioactive glass throughout the resin. The primary purpose of this research was to determine the crystalline phases present and to analyze whether the nanoparticles maintained their structural integrity post-incorporation. The test enabled the determination of crystallite size (D) using the Scherrer equation, which revealed the physical properties of the implanted particles.

Fourier Transform Infrared spectroscopy with Attenuated Total Reflectance (FTIR-ATR)

Fourier Transform Infrared spectroscopy with Attenuated Total Reflectance (FTIR-ATR) was performed with a Spectrum Two spectrometer (PerkinElmer Inc., USA). The investigation was done over the range of 4000–400 cm^{-1} to identify the functional groups contained in the bioactive glass nanoparticles. Specimens were positioned directly on the ATR crystal, and spectra were obtained to reveal the specific vibrational bands associated with silicate-based materials for pure BAG nanoparticles and 3D-printed acrylic resin comprising 3 wt% BAG.

Field Emission Scanning Electron Microscope (FESEM)

Applying a Field Emission Scanning Electron Microscope (ZEISS Sigma VP, Germany) with a spatial resolution of approximately 1.5 nm, the surface morphology and nanoparticle distribution were investigated. One specimen from each group was chosen for imaging. To improve conductivity, a sputter coater was employed to apply a thin gold coating (approximately 20 μm). Under an accelerating voltage of 15 kV, micrographs were captured at magnifications ranging from 2000× to 5000×.

Mechanical tests of specimens

Flexural strength test

For evaluating flexural strength, a total of 60 specimens (ten per group) were prepared. Testing was carried out using a three-point bending setup on a Universal Testing Machine (Cussons, England) with a 50 mm span and a 5 kN load applied at a crosshead speed of 5 mm/min[24]. The diameter of the support was 3.2 mm. The flexural strength (σ) was determined in megapascals (MPa) using the standard formula, and the maximal load at fracture was recorded in Newtons (N).

$$\sigma = \frac{3FL}{2bd^2}$$

The fracture load is denoted by F in Newtons, the span length between supports is L in millimeters (50 mm), the specimen width is b in millimeters, and the specimen thickness is d in millimeters.

Surface roughness test

Surface roughness was measured using a portable tester (SRT-6200, Guangzhou Landtek Instruments Co., Ltd., China)[25]. The device recorded the surface irregularities on an 11 mm trace length. Measurements of three actions were taken in different directions on each specimen, and the mean value was recorded in micrometers (μ).

Surface hardness test

Surface hardness was measured using a digital Shore D durometer[26]. Tests were conducted using a conical indenter (SR 0.1 mm, 30) with a constant load of 44.5 N. For each specimen, measurements were taken at three points, each 2 mm in diameter, around the center. The mean had been taken as the total Shore D hardness value.

Statistical analysis

Data analysis was done using SPSS 25 (IBM Corp., Armonk, NY, USA). To determine whether the specimens followed a normal distribution, the Shapiro-Wilk test was performed. The result indicated that flexural strength and surface hardness data were normally distributed. Resting on this result, one-way analysis of variance (ANOVA) was used to compare the groups, and pairwise comparisons were implemented with the Tukey HSD post hoc test to determine statistical differences. Nonetheless, the results on surface roughness failed to align with the concept of normality.

Hence, instead of the parametric ANOVA, the non-parametric Kruskal-Wallis test was applied to compare the groups, followed by the Mann-Whitney U test for pairwise comparisons. A significant level of $p < 0.05$ was considered for all statistical tests.

Results

Characterization results

X-Ray Diffraction (XRD) analysis

The structural characteristics of pure BAG nanoparticles were identified, and their addition to a 3D-printed acrylic resin matrix containing 3% BAG was examined using XRD analysis. The diffractogram of the pure BAG (Figure 1A) showed a broad hump centered at $2\theta \approx 31.5°$, along with low-intensity broad peaks between 20° and 36°, indicative of an amorphous structure typical of bioactive glass. Minor crystalline reflections at approximately $2\theta \approx 26.5°$ indicate the presence of unreacted crystalline phases most likely arising during precursor materials or partial devitrification.

The X-ray diffraction pattern of composite resin with 3% BAG (Figure 1B) shows sharp peaks at 2θ values of 26.6°, 28.7°, and 31.1°, with the peak at 28.7° exceeding 7000 counts. Narrow full-width at half maximum (FWHM) readings and elevated peak intensities signify an increased level of crystallinity. This indicates that the BAG nanoparticles were effectively integrated into the resin matrix without structural deterioration. The appearance of crystalline characteristics may indicate partial crystallization or structural reorganization of the BAG particles, which can be triggered by thermal or photopolymerization conditions during 3D printing and post-curing.

Fourier Transform Infrared Spectroscopy (FTIR-ATR)

The analysis of BAG nanoparticles by FTIR-ATR (Fig. 2A) showed distinctive absorption bands indicative of their functional groups and structural composition. A significant signal at 3430.76 cm^{-1} implies O–H stretching, indicating the presence of surface hydroxyl groups or moisture. The band at 2925.69 cm^{-1} was ascribed to C–H stretching, presumably from residual organics. A peak at 1650.54 cm^{-1} corresponds to H–O–H bending, indicating the presence of adsorbed water.

A distinct band at 1032.32 cm^{-1}, associated with Si–O–Si asymmetric stretching, verified the silicate framework. The bending modes of Si–O–Si and Si–O, respectively, were shown to be responsible for the supplementary peaks that were observed at 733.08 cm^{-1} and 495.07 cm^{-1}, respectively. A slight rise at 2345.88 cm^{-1} may indicate the presence of carbonate species or ambient carbon dioxide. The spectrum confirmed the characteristic silicate structure of bioactive glass and structural integrity.

The spectrum obtained from FTIR-ATR of 3D-printed acrylic resin modified with BAG nanoparticles (Fig. 2B) exhibited characteristic peaks of both the nanoparticles and the resin. A prominent band at 3434.73 cm^{-1} signified O–H stretching, whereas peaks at 2957.09, 2925.05, and 2854.57 cm^{-1} were attributed to C–H stretching from PMMA. The C=O stretching band was observed at 1730.66 cm^{-1}, while a peak at 1632.72 cm^{-1} indicated H–O–H bending, indicating the presence of adsorbed moisture.

The characteristic peaks of both the resin and the glass were observed in the FTIR-ATR spectrum of the 3D-printed acrylic resin modified with BAG nanoparticles (Fig. 3B). Although three maxima at 2957.09, 2925.05, and 2854.57 cm^{-1} were attributed to C–H stretching in PMMA, a broad band at 3434.73 cm^{-1} was an indication of O–H stretch. The C=O stretching band was seen at 1730.66 cm^{-1}, and a peak representing H–O–H bending (indicative of adsorbed moisture) was seen at 1632.72 cm^{-1}.

Notably, absorption bands between 1250 and 1115 cm^{-1} and in the 700–500 cm^{-1} range confirmed the presence of Si–O–Si and Si–O vibrations from the BAG network. These findings indicate the successful integration of BAG into the resin without altering the polymer's structure.

Field Emission Scanning Electron Microscope (FESEM)

The control group had a homogeneous surface composition, with no nanoparticles present on the surface (0% BAG). In BAG-modified specimens, surface morphology exhibited variation with concentration. At a concentration of 1%, nanoparticles were uniformly distributed with minimal evidence of agglomeration. The 1.5% and 2% groups showed the most advantageous distribution, characterized by uniform dispersion and negligible clustering. While distinct localized aggregations formed at 2.5% and 3%, they were limited in scope and did not significantly impact the overall homogeneity of the composite resin structure. The findings indicate that BAG concentrations of up to 3% can be efficiently integrated into the resin matrix with minimum agglomeration, preserving structural integrity and distribution quality.

The control group (0% BAG): A smooth, uniform surface that lacks any particulate matter.

1% BAG: The nanoparticle distribution is inadequate yet detectable.

1.5% BAG: Particles that are well-dispersed and have optimal integration throughout the matrix.

2% BAG: A homogeneous dispersion with little agglomeration and well-integrated particles.

2.5% BAG: Onset of small localized aggregation.

3% BAG: Clustering is evident in the early stages; however, agglomeration is limited and does not significantly alter the matrix structure.

Flexural strength

The groups with different amounts of bioactive glass did not exhibit statistically significant changes in flexural strength ($p = 0.527$). The average flexural strength varied from 130.45 ± 2.43 MPa in the control group to 135.45 ± 2.01 MPa in the 3% BAG group, with intermediate values obtained for the remaining concentrations. The comprehensive range among all groups ranged from 126.0 to 139.0 MPa (Table 2).

A slight increase in mean flexural strength was observed with increasing BAG concentrations, particularly in the 1.5% and 3% groups; however, these differences did not reach statistical significance.

Surface hardness

The mean and standard deviation of surface hardness values for all acrylic sample groups are summarized in Table 3.

While no overall statistically significant difference in surface hardness was found among the groups ($p > 0.05$), Group C (1.5%, 89.87 ± 1.20) and Group D (2%, 89.93 ± 1.15) showed significantly higher hardness compared to the control group (88.18 ± 1.57), with p-values of 0.028 and 0.020, respectively. None of the other group comparisons was found to be statistically significant. The most significant improvements in surface hardness occurred at concentrations of 1.5% and 2% bioactive glass.

Surface roughness

The mean and standard deviation of surface roughness values for all acrylic sample groups are presented in Table 4. Whereas the Kruskal-Wallis test revealed no statistically significant overall difference in surface roughness between the groups ($H = 10.686$, $p = 0.058$), a trend of decreasing surface roughness with increasing concentration of BAG nanoparticles was identified. Pairwise comparisons revealed significantly lower surface roughness in Group F (3%) compared to both Group A (0%) ($p = 0.010$) and Group B (1%) ($p = 0.014$). Group E (2.5%) also exhibited a reduction in roughness compared to the control; however, the difference was not statistically significant ($p = 0.064$). Incorporating 3% BAG nanoparticles significantly enhances surface smoothness in 3D-printed acrylic resin.

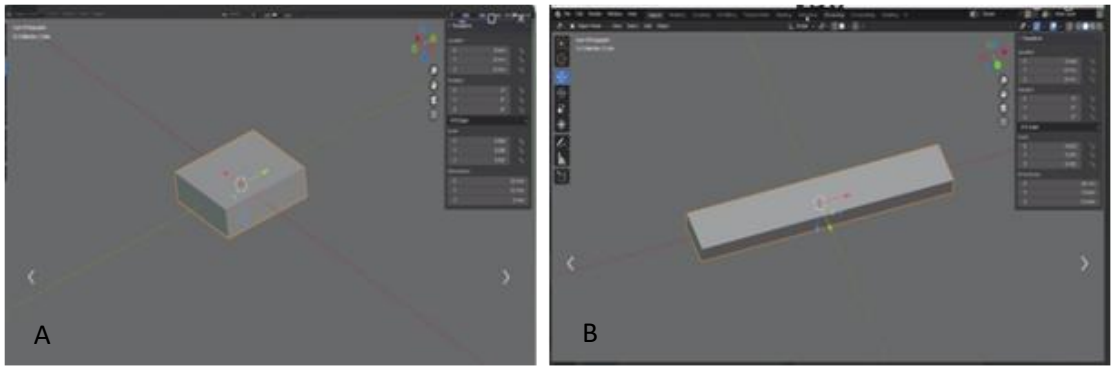

Figure 1: Screenshot of Blender software for flexural strength, surface roughness, and hardness testing, prepared for 3D printing. (A) Design of the sample used for surface roughness and hardness tests. (B) Design of the sample used for flexural strength testing.

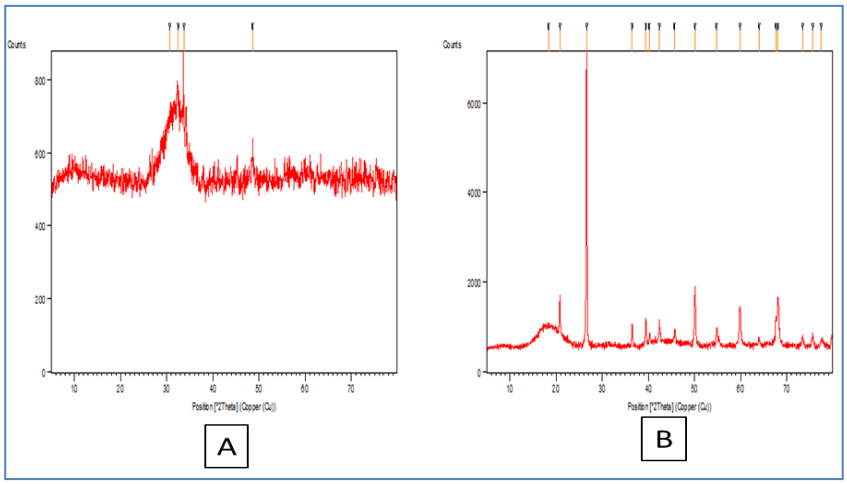

Figure 2: XRD study of BAG nanoparticles (A) and BAG-modified 3D printed acrylic resin (B).

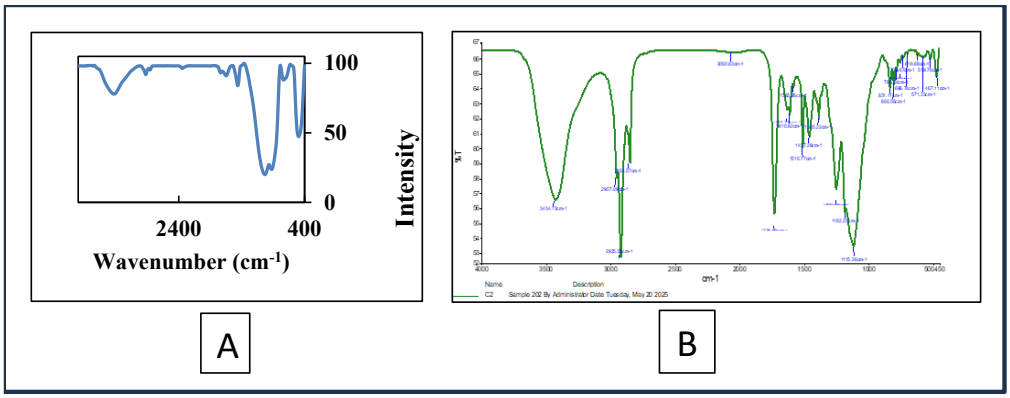

Figure 3: FTIR Spectrum of (A) BAG nanoparticles. FTIR spectrum of (B) BAG mixed with 3D acrylic resin.

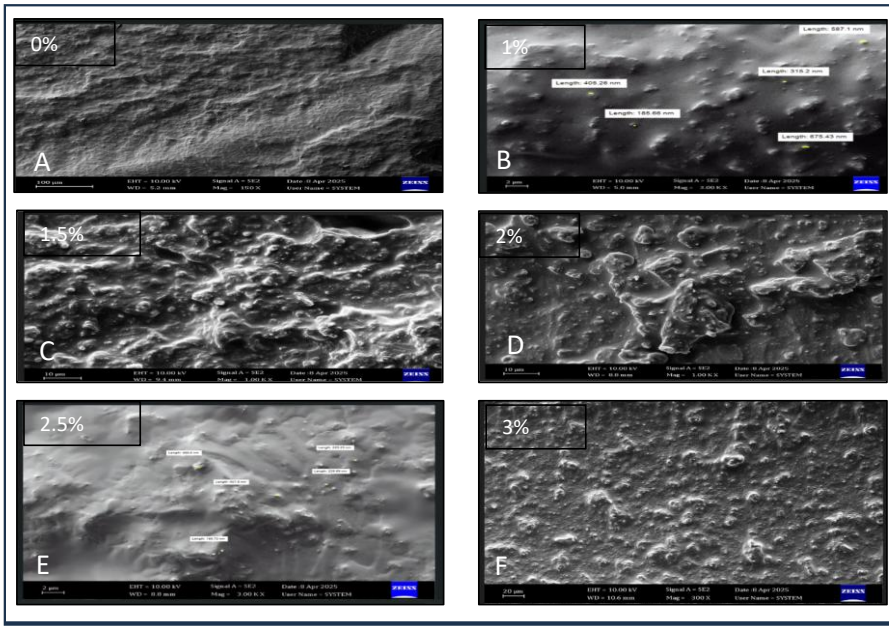

Figure 4: FESEM images of 3D-printed acrylic resin with different BAG concentrations, Surface features vary with increasing nanoparticle content.: (A) 0%, (B) 1%, (C) 1.5%, (D) 2%, (E) 2.5%, (F) 3%.

Table 1**:** Weight percent of bioactive glass nanoparticles combined with 100 cm³ of 3D-printed acrylic resin and the corresponding total mass of added bioactive glass nanoparticles and 3D resin material batch mass.

Group (n = 10)	Nanoparticle Concentration (wt%)	Density 1.2 Weight (gram)	g/cm³ Nano (gram)	Total 3D-resin batch
A (Control)	0%	120	0.0	120
B	1 wt%	120	1.8	118.2
C	1.5 wt%	120	2.7	117.3
D	2 wt%	120	3.6	116.4
E	2.5 wt%	120	4.5	115.5
F	3 wt%	120	5.4	114.6

Table 2: Flexural strength (MPa) mean, standard deviation, minimum, and maximum values.

Groups	Mean ± SD	Minimum	Maximum
A (control)	130.55 ± 2.43	126.0	135.5
B (1%)	131.69 ± 2.19	129.5	135.1
C (1.5%)	135.24 ± 2.25	132.3	139.0
D (2%)	131.06 ± 2.12	128.0	134.2
E (2.5%)	135.22 ± 2.17	132.1	138.9
F (3%)	135.45 ± 2.01	132.7	138.6

Table 3: Mean hardness (Shore D), standard deviation, minimum, and maximum values.

Groups	Mean ± SD	Minimum	Maximum
A (control) [a]	88.18 ± 1.57	85.83	91.17
B (1%)[abc]	88.68 ± 1.44	86.67	90.17
C (1.5%)[b]	89.87 ± 1.20	88.17	91.17
D (2%)[c]	89.93 ± 1.15	89.17	90.83
E (2.5%)[abc]	89.03 ± 0.89	88.00	90.50
F (3%)[abc]	88.85 ± 1.18	86.00	90.33

Note: Different superscript letters indicate statistically significant differences among groups ($p < 0.05$).

Table 4: Surface roughness (µm) mean, standard deviation, minimum, and maximum values.

Groups	Mean ± SD (µm)	Minimum (µm)	Maximum (µm)
A (control)[a]	0.134 ± 0.090	0.063	0.345
B (1%)[b]	0.125 ± 0.101	0.062	0.400
C (1.5%)[abc]	0.102 ± 0.074	0.043	0.297
D (2%)[abc]	0.076 ± 0.034	0.038	0.145
E (2.5%)[abc]	0.097 ± 0.098	0.019	0.368
F (3%)[c]	0.063 ± 0.017	0.044	0.086

Note: Different superscript letters indicate statistically significant differences among groups ($p < 0.05$).

Discussion

Structural characterization

The patterns obtained from XRD confirmed the mainly amorphous structure of BAG and partial crystallization in the composite resin, which can be attributed to reinforcement properties and stability. FTIR-ATR spectra exhibited characteristic bands of both PMMA (C–H, C=O) and BAG (Si–O–Si), with no significant chemical shifts, confirming the physical incorporation and preservation of the silicate framework. Nanoparticle distribution at different concentrations was directly proved with FSEM observations. The specimen in the control group had an even surface. In contrast, BAG-modified specimens were evenly distributed at 1.5-2% and marginally agglomerated at higher loadings.

Currently, there is a notable lack of published research specifically addressing the incorporation of bioactive glass nanoparticles into 3D-printed denture base resins and their influence on physical and mechanical properties. Hence, the interpretation of this study's results largely relies on comparisons with studies that involve conventional heat-polymerized polymethyl methacrylate (PMMA) or silica-based nanoparticles, as most BAG formulations have a high silica composition. Although the differences in the composition and processing technique of resins have been identified, these previous investigations constitute the key to understanding the reinforcement mechanism of nanoparticles in the dental polymer system. In the study, higher loadings (>5%) were avoided to prevent agglomeration, decreased mechanical strength, and poor polymerization, ensuring printability and homogeneous nanoparticle dispersion[2,21].

Flexural strength

Although flexural strength values showed a slight increase with rising BAG concentrations, these differences did not reach statistical significance. This may indicate a potential trend toward improved mechanical performance; however, such interpretation should be considered with caution and cannot be regarded as clinically conclusive without stronger statistical support. This enhancement can be attributed to the quantitative analysis of nanoparticle filler activity, resulting in enhancing the integrity of the polymer matrix by diminishing microdefects and preventing crack formation[27,28].

It has been shown that solid nanoparticles Silicon dioxide and Titanium dioxide improve stress distribution and crack resistance in PMMA when incorporated. The increase is primarily related to their improved percentage, which facilitates activities such as fracture bridging, energy dotting, and robust interfacial bonding with the resin latticework[29]. Nevertheless, excessive filler loading is well-documented to cause matrix saturation, leading to stress concentration zones and a subsequent decline in mechanical performance[30].

Moreover, numerous studies indicate that substantial enhancements in flexural strength generally occur at elevated nanoparticle concentrations, frequently above 5%, when the filler content significantly influences the material's mechanical function[19,20]. Studies on BAG-affected acrylic resins suggest that at high concentrations (e.g., 20%), such products can support flexural strengths above 65 MPa, therefore meeting the ISO 20795 qualification requirements of denture base use[22]. These studies show the potential of BAG as a reinforcing additive for increasing its mechanical properties. The study indicates that the tested concentrations (1–3%) yield a moderate yet continuous improvement in flexural strength, confirming their appropriateness as reinforcement agents in 3D-printed resin systems.

Surface hardness

The addition of BAG resulted in a significant enhancement of surface hardness at concentrations of 1.5% and 2%. The increased performance could have been due to the uniform dispersion of nanoparticles, which may have filled microvoids in the polymer matrix and restricted the mobility of polymer chains, resulting in a denser and more rigid structure[31].

These results align with the most recent studies on silica nanoparticle-reinforced acrylic polymers, which suggest that a broader nanoparticle distribution is associated with improved mechanical performance. The maximum values were observed at 5% loading, and surface hardness continued to improve as silica content increased[32].

Similar trends have been observed in composites that are reinforced with zirconia and aluminum oxide (Al_2O_3) nanoparticles. The surface hardness of PMMA substantially increased at nanoparticle concentrations of 2.5% and 5%, a phenomenon that is linked to the enhancement of interfacial adhesion and the formation of a more compact polymer-filler network[30,33].

These data highlight that nanoparticle composition, concentration, and dispersion quality are key determinants influencing the surface hardness of dental resin composites.

Surface roughness

Denture base materials that produce desirable surface roughness are recommended to make dentures last

longer and inhibit the attachment of microbes on the surface[34]. The increase in BAG was observed to decrease the degree of surface roughness of 3D-printed denture base resin. A 3% concentration was observed to significantly improve the degree of surface roughness compared to 0% and 1% concentrations. The outcomes demonstrate that a greater quantity of BAG nanoparticles might cover the small surface pores and seal the outer surface.

In contrast, an earlier study had suggested that there may be a slight increase in the roughness of conventional acrylic resin surface with high levels of BAG (up to 20%), which could be due to the polymerization technique and leaching out of residual monomer and some soluble particles, leaving void areas responsible for changes in surface roughness[13].

Conversely, a significant reduction of the roughness was noted at the BAG concentration of up to 3%, meaning that the lower concentration ratio is effective in terms of enhancing the surface (by filling the irregularities of the surface) without creating any aggregations and other defects of the surface.

The results confirm the significant effect of both the concentration and distribution of BAG nanoparticles on the final surface characteristics of the resin. Importantly, smoother denture base surfaces are less prone to microbial adhesion and plaque accumulation, which suggests that the reduced roughness achieved with BAG incorporation may contribute to antifouling effects and enhanced long-term clinical performance of dentures.

Although the bioactivity of BAG has been well established in earlier studies, this work did not include direct validation tests such as ion release, pH change, or apatite formation. Similarly, artificial aging protocols (thermocycling, water storage, or mechanical fatigue) were not performed, so the results mainly reflect short-term mechanical behavior. Future study incorporating these methods will help confirm the clinical relevance of BAG-modified 3D-printed denture base resins.

Conclusion

The incorporation of BAG nanoparticles into the 3D-printed denture base resin enhances mechanical and physical characteristics. There was a non-significant progressive increase in flexural strength with rising BAG concentrations. Elevated BAG concentrations, particularly at 1.5% and 2%, markedly improve surface hardness. As the concentration of BAG nanoparticles increased, a gradual reduction in surface roughness was observed, indicating an improvement in surface quality.

References

1. Rezaie F, Dahri M, Farshbaf M, Masjedi M, Maleki R, Amini F. 3D printing of dental prostheses: Current and emerging applications. J Compos Sci. 2023;7(2):80.
2. Ataei K, Ghaffari T, Moslehifard E, Dizaj SM. Physico-chemical and mechanical assessments of a new 3D printed PMMA-based acrylic denture base material. Open Dent J. 2024;18(1):1-6.
3. Karni PA, Maheshwari S, Sarada V, Dass SS, Ananda MN. 3D printing in dentistry: revolutionizing customization and delivery of dental prosthetics. J Neonatal Surg. 2025;14(4):473-8.
4. Dimitrova M, Corsalini M, Kazakova R, Vlahova A, Chuchulska B, Barile G, et al. Comparison between conventional PMMA and 3D printed resins for denture bases: A narrative review. J Compos Sci. 2022;6(3):87.
5. Qadir GO, Abdulkareem JF. An in vitro comparative study of maxillary denture base retention between conventional fabrication and 3D printed techniques. Sulaimani Dent J. 2023;10(2):45-53.
6. Alhotan A, Yates J, Zidan S, Haider J, Silikas N. Flexural strength and hardness of filler-reinforced PMMA targeted for denture base application. Materials (Basel). 2021;14(10):2659.
7. Al-Douri ME, Sadoon MM. Flexural strength, hardness and surface roughness of 3D printed denture base resin reinforced by zinc oxide nanoparticles. J Res Med Dent Sci. 2023;11(1):194-200.
8. Sodagar A, Bahador A, Khalil S, Shahroudi AS, Kassaee MZ. The effect of TiO_2 and SiO_2 nanoparticles on flexural strength of poly (methyl methacrylate) acrylic resins. J Prosthodont Res. 2013;57(1):15-9.
9. Altarazi AT, Jadaan L, McBain AJ, Haider J, Kushnerev E, Yates J. 3D-Printed nanocomposite denture base resin: The effect of incorporating TiO_2 nanoparticles on the growth of Candida albicans. J Prosthet Dent. 2023;130(2):283-9.
10. Altarazi AT, Haider J, Alhotan A, Silikas N, Devlin H. 3D printed denture base material: The

effect of incorporating TiO_2 nanoparticles and artificial ageing on the physical and mechanical properties. J Mech Behav Biomed Mater. 2023;39(10):1122-36.
11. Majeed HF, Hamad TI, Bairam LR. Enhancing 3D-printed denture base resins: A review of material innovations. Sci Prog. 2024;107(3):368504241263484.
12. Aati S, Akram Z, Ngo HC, Fawzy AS. Development of a 3D-printed denture-base resin einforced with silver/zinc oxide mesoporous nanoparticles: mechanical, biological and antibiofilm properties. J Mech Behav Biomed Mater. 2022;134:105418.
13. Alhotan A, Raszewski Z, Chojnacka K, Mikulewicz M, Kulbacka J, Alaqeely R, et al. Evaluating the translucency, surface roughness, and cytotoxicity of a PMMA acrylic denture base reinforced with bioactive glasses. J Funct Biomater. 2024;15(1):16.
14. Jones JR. Review of bioactive glass: From Hench to hybrids. Acta Biomater. 2013;9(1):4457-86.
15. González P, Serra J, Liste S, Chiussi S. Raman spectroscopic study of bioactive silica based glasses. J Non Cryst Solids. 2003;320(1–3):92-9.
16. Misra SK, Mohn D, Brunner TJ, Stark WJ, Philip SE, Roy I. Comparison of nanoscale and microscale bioactive glass on the properties of P(3HB)/Bioglass® composites. Biomaterials. 2008;29(12):1750-61.
17. Liu S, Gong W, Dong Y, Hu Q, Chen X, Gao X. The effect of submicron bioactive glass particles on in vitro osteogenesis. RSC Adv. 2015;5(49):38830-6.
18. Al-Eesaa NA, Johal A, Hill RG, Wong FS. Fluoride-containing bioactive glass composite for orthodontic adhesives: apatite formation properties. Dent Mater. 2018;34(8):1127-33.
19. Raszewski Z, Chojnacka K, Kulbacka J, Mikulewicz M. Mechanical properties and biocompatibility of 3D printing acrylic material with bioactive components. J Funct Biomater. 2023;14(1):13.
20. Raszewski Z, Chojnacka K, Mikulewicz M. Preparation and characterization of acrylic resins with bioactive glasses. Sci Rep. 2022;12(1):16624.
21. Raszewski Z, Nowakowska D, Wieckiewicz W, Nowakowska A. Release and recharge of fluoride ions from acrylic resin modified with bioactive glass. Polymers (Basel). 2021;13(7):1054.
22. Raszewski Z, Chojnacka K, Mikulewicz M, Alhotan A. Bioactive glass-enhanced resins: A new denture base material. Materials (Basel). 2023;16(12):4363.
23. Prpić V, Schauperl Z, Ćatić A, Dulčić N, Čimić S. Comparison of mechanical properties of 3D-printed, CAD/CAM, and conventional denture base resins. J Prosthodont. 2020;29(6):524-8.
24. Raouf L, Faraj S, Azhdar B. Evaluation of flexural strength of heat cure PMMA denture base material reinforced with various concentrations of zirconium oxide. Sulaimani Dent J. 2019;6(2):22-30.
25. Rashid AAL. Some properties of 3D printed acrylic resin material modified by antifungal Vitis vinifera oil. Dent 3000. 2025;1:a001.
26. Gaviria-Martinez A, Castro-Ramirez L, Ladera-Castañeda M, Cervantes-Ganoza L, Cachay-Criado H, Alvino-Vales M, et al. Surface roughness and oxygen inhibited layer control in bulk-fill and conventional nanohybrid resin composites with and without polishing: in vitro study. BMC Oral Health. 2022;22:258.
27. Sasaki Y, Nishizawa Y, Watanabe T, Kureha T, Uenishi K, Nakazono K, et al. Nanoparticle-based tough polymers with crack-propagation resistance. Langmuir. 2023;39(26):9262-72.
28. McCabe JF, Walls AWG. Applied Dental Materials. 9th ed. Chichester (UK): John Wiley and Sons; 2013.
29. Sun L, Gibson RF, Gordaninejad F, Suhr J. Energy absorption capability of nanocomposites: A review. Compos Sci Technol. 2009;69(14):2392-409.
30. Asopa V, Suresh S, Khandelwal M, Sharma A, Saimbi CS, Mathur S. A comparative evaluation of properties of zirconia reinforced high-impact acrylic resin with that of high-impact acrylic resin. J Clin Diagn Res. 2015;9(3):ZC16-9.
31. Rahman MM, Khan KH, Parvez MMH, Irizarry N, Uddin MN. Polymer nanocomposites with optimized nanoparticle dispersion and enhanced functionalities for industrial applications. Processes. 2025;13(4):994.
32. Jayasoman S, Perera DJ, Kodagoda K. Effect of silica nanoparticles on flexural strength and surface hardness of heat polymerized acrylic resin. Bangladesh J Med Sci. 2024;23(10):S79-86.
33. Vojdani M, Bagheri R, Khaledi AAR. Effects of aluminum oxide addition on the flexural strength, surface hardness, and roughness of heat-polymerized acrylic resin. J Dent Sci. 2012;7(3):238-44.
34. Kurzendorfer-Brose L, Rosentritt M. The effect of manufacturing factors on the material properties and adhesion of Candida albicans and Streptococcus mutans on additive denture base material. Materials (Basel). 2025;18(6):1234.